ACS Biomaterials SCIENCE & ENGINEERING

pubs.acs.org/journal/abseba

Article

Design of a Ratiometric Plasmonic Biosensor for Herceptin Detection in HER2-Positive Breast Cancer

Neda Shahbazi, Rouholah Zare-Dorabei,* and Seyed Morteza Naghib

Cite This: *ACS Biomater. Sci. Eng.* 2022, 8, 871−879

Read Online

ACCESS | Metrics & More | Article Recommendations | Supporting Information

ABSTRACT: Breast cancer is the most common cause of cancer death in women; therefore, its early detection and treatment are crucial. To achieve this goal, we designed an optical sensor based on direct interaction of trastuzumab [Herceptin (HER)], a monoclonal antibody used to treat HER2-positive breast cancer, with plasmonic nanoparticles. Surface-modified gold nanoparticles (AuNPs) have gained considerable attention in biosensing techniques over the last years, which actuated these nanoparticles to the heart of various biosensing notions. We have exploited the localized surface plasmon resonance (LSPR) of gold nanoparticles to determine HER in human serum. AuNPs were decorated with negatively charged citrate ions, yielding enhanced direct-surface interaction with HER antibodies. The AuNPs are mixed with silver nanoparticles (AgNPs) in an optimized ratio to increase selectivity and sensitivity further. AuNPs detect the HER antibodies using LSPR, whereas AgNPs help monitor interferences' effect on the sensing media. The three effective factors in HER sensing, including the nanoparticle ratio, temperature, and pH were optimized via response surface methodology (RSM) based on the central composite design (CCD). The sensor's response toward HER was achieved in the linear range of 0.5×10^{-7} to 40×10^{-7} M with the detection limit of 3.7×10^{-9} M and relative standard deviation (RSD) less than 5%. The selectivity of the LSPR sensor was assessed by monitoring its response toward HER in the presence of other biological molecules with similar physicochemical properties. Rapid response time (less than 1 min), selectivity, and the simplicity of the developed LSPR-based sensor are the key advantages of the developed sensor.

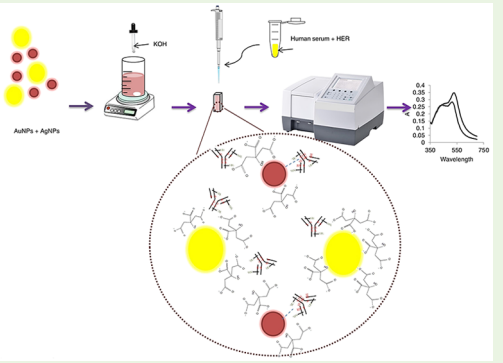

KEYWORDS: *localized surface plasmon resonance (LSPR), gold nanoparticles (AuNPs), silver nanoparticles (AgNPs), Herceptin detection, nanobiosensor, breast cancer*

INTRODUCTION

Cancer-related antigen−antibody interactions are frequently used in diagnosis, treatment, and determination of prognosis of cancers in clinical trials. It has been well appointed that HER2, a monoclonal antibody that binds to the extracellular domain (ECD) of the HER2/neu receptor, exhibits considerable expression in breast cancers (BC), serving as a potential biomarker and a detecting agent in therapeutic and prognostic case studies.[1−7] Human BC that has an overexpressed level of HER2 protein is mentioned as HER2-positive BC. HER2-positive BC commonly develops and spreads more rapidly than other BCs, and its metastatic forms are incurable, and new treatment methods are desired. The higher HER2 is expressed, the lower is the survival chance and the higher is the possibility of metastases. Thus, demand has increased for improvements in cancer biomarker screening and detection. The American Society of Clinical Oncology (ASCO)/College of American Pathologists (CAP) published the guidelines on HER2 clarification to offer defined instructions for precise determination of HER2 levels in BC.[5,8,9] Up to now, various analysis platforms have been documented for the rapid detection of BC biomarkers such as immunohistochemistry (IHC),[3] fluorescence in situ hybridization (FISH),[9] and chromogenic in situ hybridization (CISH)[9] like silver in situ hybridization (SISH),[9] which are regarded as standard methods in clinical study and some other biochemical-based analysis including enzyme-linked immunosorbent assay (ELISA),[10] optofluidic ring resonator (OFRR),[11] ring resonator sensor and surface acoustic wave (SAW), electrochemical (EC),[2,12,13] surface-enhanced Raman scattering (SERS),[14] fluorescence,[1,15−18] and colorimetric analysis.[19] However, some of these methods are based on multipart manufacturing procedures, limiting their usage due to expensive equipment[15] and high methodological expertise.[3,10,15] Regardless of the mentioned analysis methods, it should be noted that early and adjusted anticancer therapies with greater effectiveness of BC are just as crucial as its early recognition. The detection of BC and medical intervention

Received: October 27, 2021
Accepted: January 6, 2022
Published: January 19, 2022

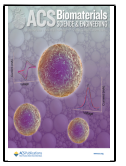

before the metastatic stage could promote the survival chance and improve the quality of patient life. The innovation of monoclonal antibodies against the ECD of the HER2 protein was considered a fundamental step forward in anti-BC therapies. Trastuzumab [Herceptin(HER)] was the initial humanized monoclonal antibody introduced by the Food and Drug Administration (FDA) of the USA in 1998 and the European Medicines Agency (EMA) 2 years later for the treatment of not only in early-stage but also in metastatic HER2 overexpressing BC. Some procedures have the key aims to recognize programs involving the management of trastuzumab loading doses on uninterrupted days to cause therapeutic concentration levels during a shorter time.[8,20]

Consequently, monitoring and screening this drug in body fluids have gained significant attraction. In this field, localized surface plasmon resonance (LSPR)-based analysis methods are fast and straightforward. Indeed, the advent and commercialization of these plasmonic sensing platforms are recently beginning to expand under their improved reproducibility and unique optical features, which may compensate for the shortcomings of other methods. In addition, the integration of plasmonic biosensors with the upcoming equipment technologies will help improve the healthcare outcome.[21] Over the recent decades, applications of different plasmonic nanomaterials like gold,[22−27] silver,[11,28−30] and platinum[31,32] in BC clinical diagnostic methodologies and therapy have been reported in several studies, which can result in forming the idea that the innovation of plasmonic nanobiosensors merges the advantages of optical biosensing with nanotechnology, thereby creating a new type of low cost and ultrasensitive diagnostics.[24] It is generally accepted that these novel plasmonic nanobiosensors are able to fulfill the shortcomings of the conventional detection techniques.[21]

The valuable characteristics of AuNPs, such as their simplicity of synthesis and various surface functionalization mechanisms indicating why gold nanoparticles, are an attractive candidate for further improvement in the clinical diagnosis method, which is thoroughly described in a review article by Gambhir.[33] AuNP-based nanobiosensors are developed as substitutes and facile tools for improving highly sensitive biosensors because of their proper conjugation procedure and superior optical and electrical features.[25,34−37] Also, the LSPR-based technique receives promoting interest because of its wide applications in catalysis, phototherapy, and cellular imaging.[38−40] In these tools, when AuNPs with particular decorating groups identify their targets, the interaction between both molecules causes a local deviation in the refractive index at the metal surface, which can be screened by spectrometric analysis.

Real-time monitoring, high selectivity, and sensitivity are some distinct advantages of LSPR-based sensing methods, allowing us to develop an affordable, easy-to-use nanobiosensor for HER detection based on AuNPs. To screen unwanted interferences, a mixture of AuNPs and AgNPs in an appropriate volume ratio was selected as a sensing component, given that the distinct LSPR spectra of the two nanoparticles are in the visible region. The presence of AgNPs in the sensing solution would be beneficial as the observer species to take advantage of the ratiometric sensing platform. Spectral analysis revealed no noticeable change in the LSPR intensity and the position of AgNPs toward the addition of different concentrations of HER, so the AgNPs intensity variation is considered constant in each test. Also, it makes it possible to differentiate the HER-specific interactions with AuNPs. The ratio between the changes in the intensity of AuNPs spectra (ΔI_{AuNPs}) and the constant absorbance of AgNPs (I_{AgNPs}), $(\Delta I_{AuNPs})/(I_{AgNPs})$, showed a correlation with the concentration of HER in both simulated and real samples. The outer layer of both nanoparticles is decorated by negatively charged citrate ions, promoting their interaction with the amine group of HER molecules via electrostatic interactions. In addition, the optimization of this interaction is done via monitoring the effect of three parameters of pH, temperature, and the AuNPs/AgNP volume ratio. Following the optimization of the biosensing parameters, the optimum values are adopted for further biosensing experiment, including the calibration plot of the nanobiosensor and real-sample trials. The procedure involved in this sensing is simple, cost-effective, and rapid, with no need for a skilled person or complex pieces of equipment.

MATERIALS AND METHODS

Materials. Trastuzumab (HER) was obtained from Aryogen Co. Gold(III) chloride trihydrate, trisodium citrate dihydrate, bovine serum albumin (BSA), silver nitrate, L-cysteine, ascorbic acid, L-arginine, glucose ($C_6H_{12}O_6$), and sodium chloride (NaCl) were purchased from Sigma-Aldrich. Human serum samples were obtained from the Tehran Heart Center laboratory (Tehran, Iran). In all experiments, ultrapure deionized (DI) water was used.

Instrumentation. Ultraviolet−visible (UV−vis) spectra were documented via a PG Instrument T80+ dual-beam UV/vis spectrophotometer in a detecting range of 350−700 nm with a wavelength accuracy of 1 nm. All sensing procedures were performed in an adapted 1.00 cm glass cuvette. Transmission electron microscopy (TEM) images were taken using a Philips-208S transmission electron microscope working under 100 kV voltages. A Horiba Scientific instrument performed the dynamic light scattering (DLS) analysis at a scattering angle of 90 in the monodispersed form. Zeta-potential tests were performed using Horiba Scientific tools at an electrode voltage of 3.8 V. The pH value was adjusted via a Mettler Toledo Co. pH meter.

Synthesis of Nanomaterials. Citrate capped-AuNPs were synthesized according to the previous literature.[36] To prepare citrate capped-AgNPs, 50 mL of 1×10^{-3} M $AgNO_3$ was heated to the boiling point. To the above solution, 5 mL of 58.7 mg trisodium citrate dihydrate solution was added dropwise and stirred vigorously. The solution was heated until the color became bright yellow, which proved the formation of nanoparticles. Then, it was removed from the heater and stirred until cooled to room temperature. Both NPs were purified using nanofilter paper to remove excess reagents. AuNPS and AgNPs were characterized via transmission electron microscopy (TEM), DLS, zeta potential, and UV−vis spectroscopy.

Fabrication of the Nanobiosensor. Following the production and filtration of AgNPs and AuNPs, a specific ratio of AuNPs and AgNPs was mixed and shaken gently. Afterward, the pH of the mixture was adjusted to 9 by adding 0.1 M KOH solution (prepared in DI water), and the resulting colloidal solution was stored at 4 °C. For the sensing procedure, 1.5 mL of the above solution was mixed with various concentrations of HER, followed by monitoring the changes in the LSPR of plasmonic nanostructures.

RESULT AND DISCUSSION

Ratiometric LSPR-Based Detection of HER by AuNPs and AgNPs. Different shapes of plasmonic nanostructures (e.g., AuNPs and AgNPs) have been widely used to identify different biomolecules, especially for BC biomarker detection.[41−45] The synthesized spherical AuNPs have been decorated with the negative citrate groups, making them available to interact with positively charged components. We

https://doi.org/10.1021/acsbiomaterials.1c01369
ACS Biomater. Sci. Eng. 2022, 8, 871−879

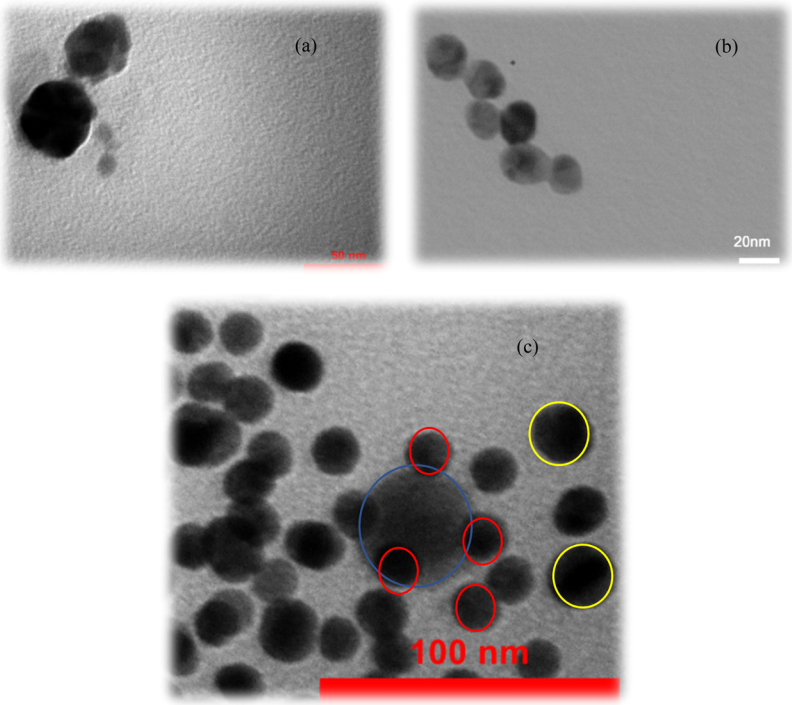

Figure 1. TEM images of AuNPs (a), AgNPs (b), and a mixture [AuNPs (red), AgNPs (yellow), HER (blue)] after the addition of HER (c).

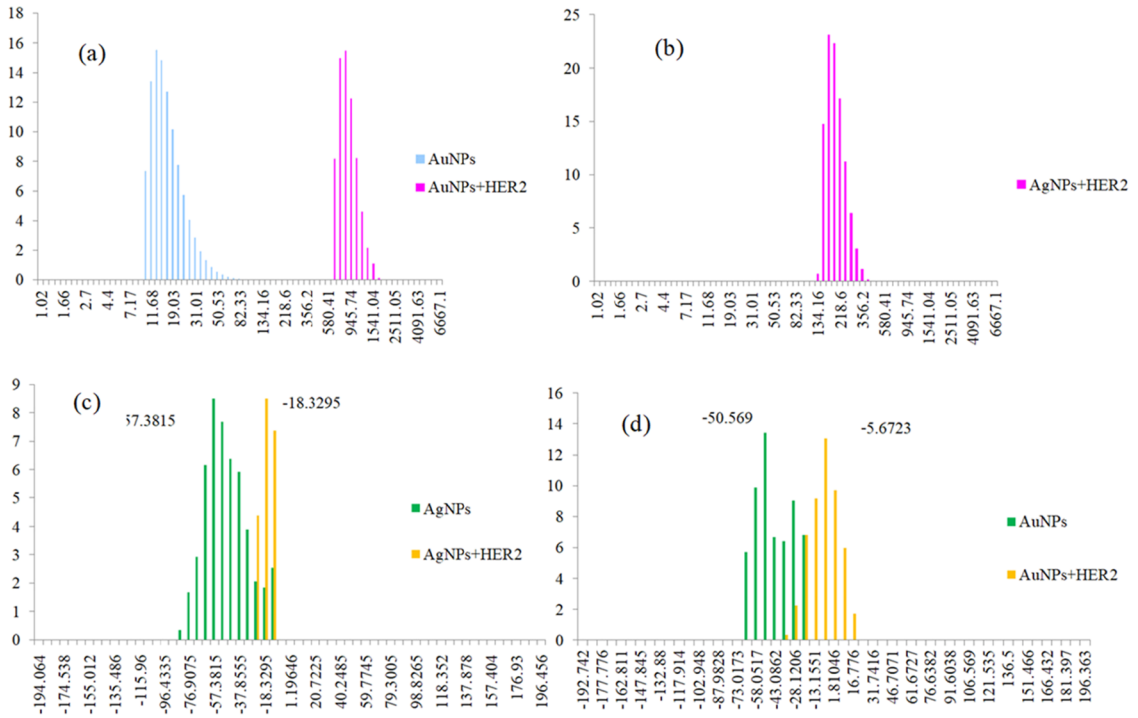

Figure 2. DLS analysis of, (a) AuNPs before and after addition of HER and (b) AgNPs after addition of HER. Zeta potential analysis of (c) AgNPs before and after addition of HER and (d) AuNPs before and after addition of HER.

have added citrate-capped AgNPs to our sensing probe to increase the selectivity. The citrate selection as the capping agent is made based on the fact that citrate has different coordinations on AuNPs and AgNPs nanoparticles previously investigated by Fourier transform infrared (FT-IR) spectroscopy and molecular orbital (MO) calculations.[46,47] AuNPs and AgNPs are found to have entirely dissimilar interactions with carboxylate anchoring groups, and the citrate ions have ionic and unidentate coordination, respectively. Consequently, more negative charges on the AuNPs can interact with trastuzumab. Up to now, some reference methods and research articles on trastuzumab detection have been verified and published.

At the moment, the enzyme-linked immunosorbent assay (ELISA) is a commonly used analytical biochemistry assay for detection biomolecules; thus, a lot of research groups promoted and modified the ELISA for specific recognition of

https://doi.org/10.1021/acsbiomaterials.1c01369
ACS Biomater. Sci. Eng. 2022, 8, 871−879

HER. In a recent work, a robust and rapid ELISA method for HER quantification *n* in human serum is suggested. Their technique is based on an antigen peptide, mimicking the portion of the HER2 receptor that interacted with HER, linked to a 96-well plate using the streptavidin/biotin system. The noted method has a detection range, between 10 and 180 μg/mL in serum. The selectivity of their sensing methodology was evaluated in the presence of bevacizumab and denosumab, two monoclonal antibodies that can be used in the BC treatment, and no cross-reactivity was observed.[48] In another similar assay, a group describes the development and validation of a cell-based ELISA to measure HER in human serum. The assay measures the interaction between HER and HER2 and has a dynamic range between 10 and 120 μg/mL.[49] These methods are comparable in terms of the detecting range with our plasmonic assay. The detection range of these ELISA tests is approximately 10^{-6} M, which is one order of magnitude greater than the assay described in this article (10^{-7} M). This result could be expected because any minor changes in the surrounding media can be detected by plasmonic nanoparticles.

Based on the two research mentioned above, it can be concluded that ELISA-based methods have several advantages, such as high specificity and reproducibility of quantitation. At the same time, ELISA performances mainly rely on antibody quality, specificity, and kit manufacturer, making them an expensive method, while our inexpensive assay has a linear range comparable to the noted ELISA method. Also, in the selectivity study, our sensor performance was tested in the presence of different components like ascorbic acid, cysteine, arginine, glucose, vitamin B, BSA, and phosphate buffer saline (PBS) with the concentration 10 times more than that of HER. In the next step, some drugs such as mercaptopurine (6-MP), carboplatin, and 4-substituted-2, 5-dimethoxyamphetamines (DOX) were selected, and their effects on the sensing system were studied. However, in the reported ELISA tests, some limited interferences are studied.

Characterization of Materials. The morphology of the obtained nanoparticles was investigated via TEM. As illustrated in Figures 1 and S1, spherical AuNPs were monodispersed with an average diameter of 14.8 nm, and the FT-IR analysis confirmed the presence of negatively charged citrate ions. In addition, the average diameter of spherical AgNPs was obtained as 50 nm. It was observed that in the presence of HER in the mixture of both NPS, the AuNPs were surrounded by HER more than AgNPs. The DLS results (Figure 2a,b) show that the size of AuNPs is approximately 14.8 nm. In contrast, after the addition of HER, the size of NPs in the solution changes to 162.5 and 802 nm for AgNPs and AuNPs, respectively, which is an indicator of the amount of aggregation in both samples. The surface charge of the nanoparticles was characterized with zeta potential. As shown in Figure 2c,d, AgNPs and AuNPs presented a sharp and intense peak of approximately −57.3 and − 50.5 mV, respectively. Furthermore, the zeta analysis illustrated the presence of negatively charged citrate ions on both nanoparticles. It was observed that after the addition of HER to AgNPs and AuNPs in DI water solution, the zeta potential peak shifted to −18.4 and − 5.6 mV, respectively, which confirmed the electrostatic interaction of HER with the NPs. The XRD pattern of the synthesized AuNPs (Figure S2) showed clear peaks of cubic phases at 38.12 (111), 44.88 (200), 64.24 (220), and 77.24 (311), which confirmed the crystalline nature of AuNPs.

Sensing Mechanism of HER. Trastuzumab (HER), which is specifically used to treat cancers that are HER2 receptor-positive, was selected as the target. This spectrophotometric nanobiosensor consists of a signal part and a capturing part. The signal unit is a mixture of AuNPs and AgNPs decorated with the capturing groups of citrate ions, capable of interacting with the HER molecules in the sample. The sensing procedure of the proposed optical nanobiosensor is illustrated in Figure 3a. In the first step, after the synthesis of citrate-capped AuNPs and AgNPs, a specific amount of both nanoparticles is mixed and adjusted to the desired pH. It should be noted that the sensing structure (AuNPs and AgNPs) contains negatively charged citrate ions, which provide a selective affinity toward the HER molecules via the positively charged functional amine group of Fc and the Fab region of HER. This ionic adsorption of antibodies on the nanoparticles' surface is favorable for the hydrophobic interactions between the hydrophobic pockets of the HER and gold. In other words, as a result of the noted ionic interaction, the HER comes close enough to AuNPs, and the hydrophobic pockets of the protein will make contact and bind with gold. These interactions are responsible for the changes in the surrounding medium of the NPs and consequently the changes in the LSPR spectra of both NPs.

Based on the spectrometric studies, the variation in the LSPR spectrum of AgNPs is negligible. However, the interactions of amine with AuNPs cause a spectral shift and intensity enhancement in the LSPR spectra. These changes showed a linear relationship with the HER concentration. Noteworthy, the color of the Ag/Au NP probe is light red, and when HER is added to this probe, the color of the mixture has no change, while the absorption intensity increases at ∼520 nm. In fact, by the addition of HER in the system, the probe-target interactions begin, so the distance between nanoparticles and the target is reduced, and consequently, aggregation occurs. Because the variation in absorption at ∼520 nm indicates the interactions of HER molecules with the AuNPs, the absorbance at ∼425 nm describes other interferences during sensing. The absorbance ratio of $(I_{AuNPs}/I_{AgNPs}) = (A_{520}/A_{425})$ can express the quantity of HER molecules. Hence, the greater A_{520}/A_{425} means higher HER concentrations in the sample.

Comparison of Sensing Responses between AgNPs and AuNPs. In this part, the interaction of HER molecules with AgNPs and AuNPs was compared. Corresponding visible spectra of both nanoparticles are shown in Figure 3b,c, which demonstrates the AgNPs' peak's intensity variation at 420 nm before and after the addition of HER. In this case, the peak intensity is constant after the addition of HER, but as shown in Figure 3b,c, the AuNP LSPR spectra at 520 nm increased and shifted.

Optimization and Statistical Analysis for HER Detection. Response surface methodology was used to optimize the effect of pH, temperature, and the nanoparticles ratio on the HER detection via Design Expert 11 software using the quadratic model under central composite design (CCD). The range of each parameter is selected based on our preliminary experiments. Twenty randomized tests in two blocks were performed, and the response of each test (I_{AuNPs}/I_{AgNPs} or A_{520}/A_{425}) is reported in the response column (Tables S1 and S2 in the Supporting Information). The predicted R^2 value of 0.778 and the adjusted R^2 of 0.922 confirm the model's adequacy (the difference is less than 0.2). The obtained value for the adequate precision was 14.086, which is

https://doi.org/10.1021/acsbiomaterials.1c01369
ACS Biomater. Sci. Eng. 2022, 8, 871−879

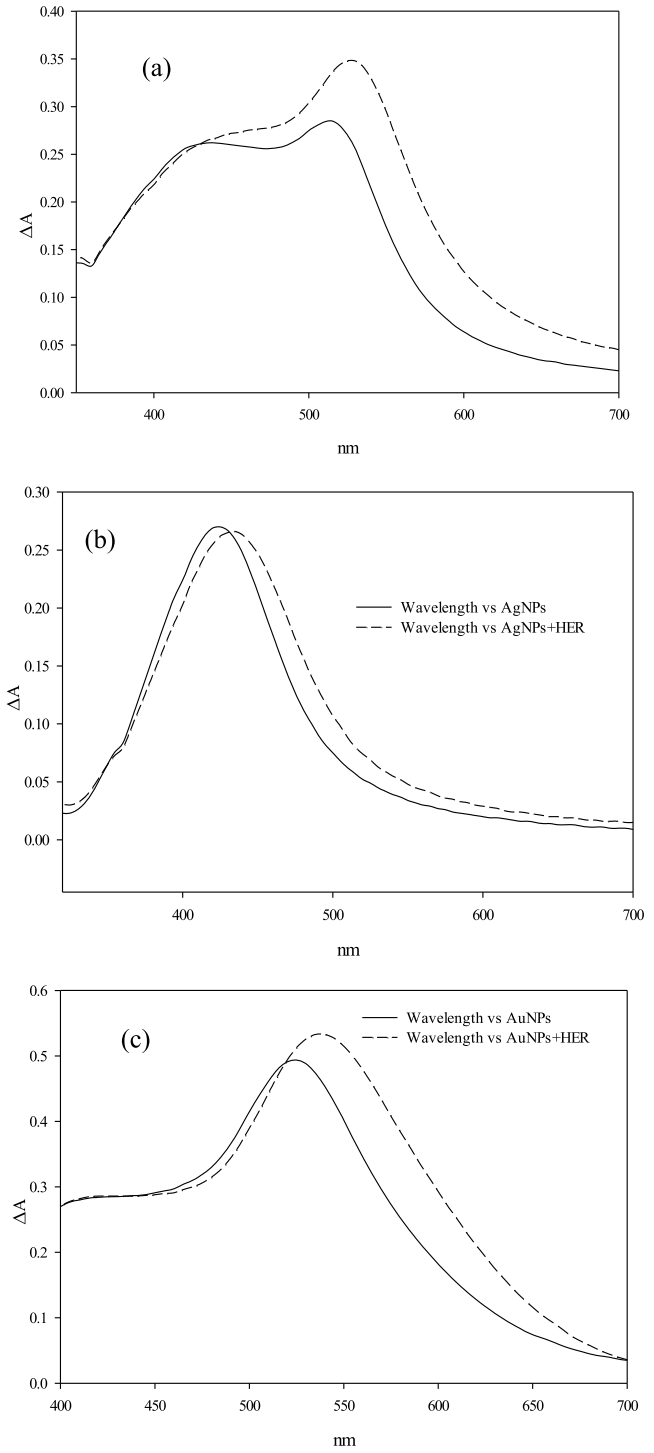

Figure 3. Nanobiosensing mechanism of the developed sensor. Panel (a) shows the LSPR spectra of AuNPs/AgNPs (ratio = 0.6) before (—) and after (---) the injection of HER. Comparing the LSPR spectra of AgNPs (b) and AuNPs (c) before (—) and after (----) the addition of HER.

greater than four, indicating an adequate signal (Table 1). Based on the result obtained from the analysis of variance (ANOVA), the amounts of the *F*-value (24.71) and the low *p*-value (< 0.0001) confirmed the significance of the model. Lack of fit (LOF) values shows the variation of data around the fitted model. If the selected model fit the analysis data well, this factor will be insignificant.

Table 1. Statistics Data of 20 Runs

std. dev.	0.1965	R^2	0.9611
mean	−4.13	adjusted R^2	0.9222
CV %	4.75	predicted R^2	0.7778
		adeq precision	14.0861

The lack of fit of the model was obtained to be 0.076, which is larger than the 0.05 critical value, indicating that the developed model is significant. Figure 4 shows the interaction between the independent variables on the response value in a surface plot. In all surface plots, one factor was kept constant while the two other factors were varied within the selected experimental ranges. It can be seen that the sensors' response decreased as the pH of the solution reached values more than 9. This behavioral pattern can be understood considering that the antibody isoelectric point (pI) is near pH = 8.5. One important characteristic of monoclonal antibodies (HER in this study) is pI, which is basically the pH at which the antibody has no net electrical charge, and its value is related to the charged amino acids the antibody contains. If the pH of the surrounding environment becomes lower than the antibody's pI, the molecule carries a net positive charge, whereas the antibody will have a net negative charge when the pH is above the pI. The response surface plots show a significant enhancement in the result via increasing the NP ratio until 0.6. As the ratio increases, more NPs can interact with HER while more than 0.6, the self-interaction between NPs can occur and may prevent the interaction between NPs and HER. For this reason, the ratio value was determined to be 0.6 for further sensing. Variations in temperature have a minor effect on the sensing result, so the optimum value in the response surface diagram is selected for this parameter. Briefly, based on the numerical results of design, the optimized value for pH, temperature, and ratio, with 0.999 desirability is 7.6, 41 °C, and 0.59, respectively, which are selected for all tests. From the optimization value of parameters in response surface diagrams (Figures S3 and S4 in the Supporting Information), it can be mentioned that each factor not only has a significant effect on sensing response but also affects the effect of other factors. In other words, each factor is involved in multiple interactions.

Selectivity and Repeatability Analysis of the Sensing Process. To explore the selectivity of the nanobiosensing method, ascorbic acid, cysteine, arginine, glucose, vitamin B, BSA, and PBS with the concentration ten times more than that of HER2 were selected as interfering agents. In the next step, some drugs such as 6-MP, carboplatin, and DOX, which have similar structures to trastuzumab, were selected, and their effects (in their original concentration) on the sensing system were studied. As shown in Figures 5 and S5, the sensing signals of cysteine, PBS, 6-MP, DOX, carboplatin, and vitamin B did not reveal a considerable increase compared with that of the HER. By contrast, when the solutions of arginine, ascorbic acid, glucose, and BSA were investigated, the sensing intensity of the nanobiosensor presented a reduced intensity in contrast with that observed after the addition of HER, which point out that the interfering molecules had negligible influence on the sensing response to HER. The repeatability of the sensor is studied by comparing the result of sensing in 7 days (Figure 6). All experimental factors like pH, temperature, and ratio were the same during 7 days. The RSD results were less than 5%.

Measurement of the Sensing Performance. To estimate the analytical performance of the reported nano-

https://doi.org/10.1021/acsbiomaterials.1c01369
ACS Biomater. Sci. Eng. 2022, 8, 871−879

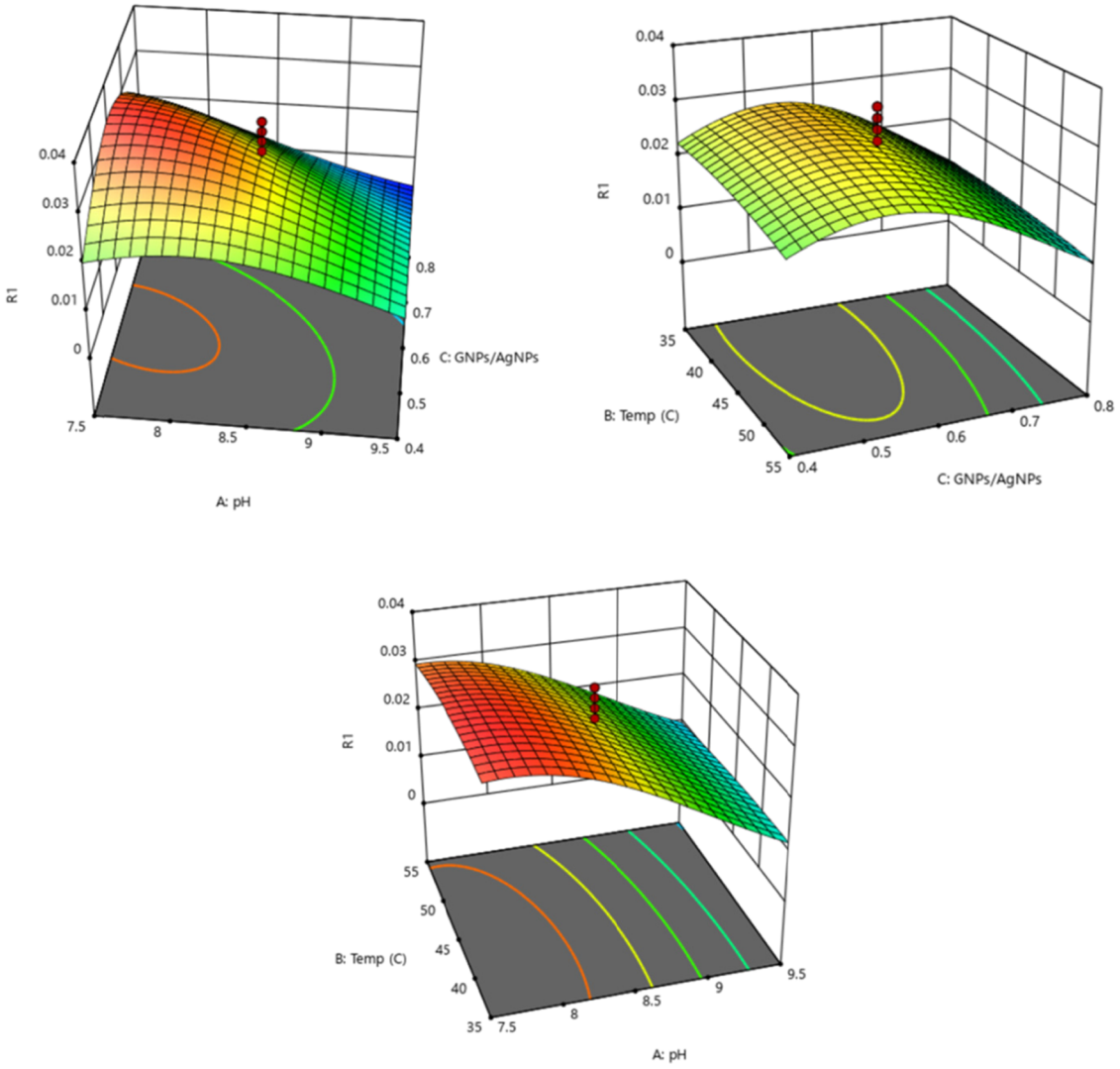

Figure 4. Response surface of two parameters.

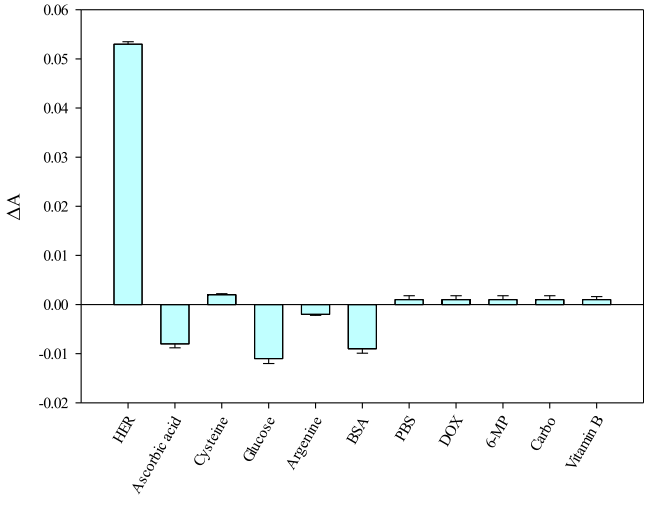

Figure 5. Selectivity of the reported sensor in the presence of other various molecules at a tenfold concentration.

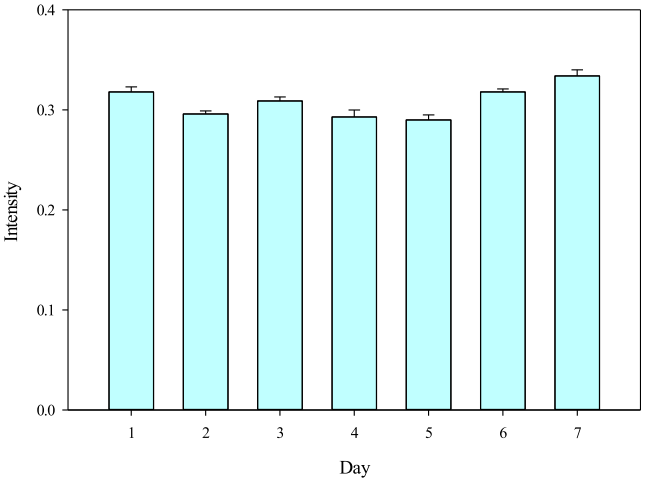

Figure 6. Repeatability of the reported sensor in 7 days.

biosensor, a wide range of HER concentrations was injected into sensing media, and the resulting variation (A_{AuNPs}/A_{AgNPs}) was measured at optimum conditions. The obtained results are shown in Figure 7. Each point in the calibration curve is the mean value of three independent tests. The limit of detection (LOD) was calculated based on $3S_b/m$ (S_b = signal of blank sample, m slope of the calibration curve). Using this method, a linear range of 0.5×10^{-7} to 40×10^{-7} M and an LOD of 3.7

https://doi.org/10.1021/acsbiomaterials.1c01369
ACS Biomater. Sci. Eng. 2022, 8, 871−879

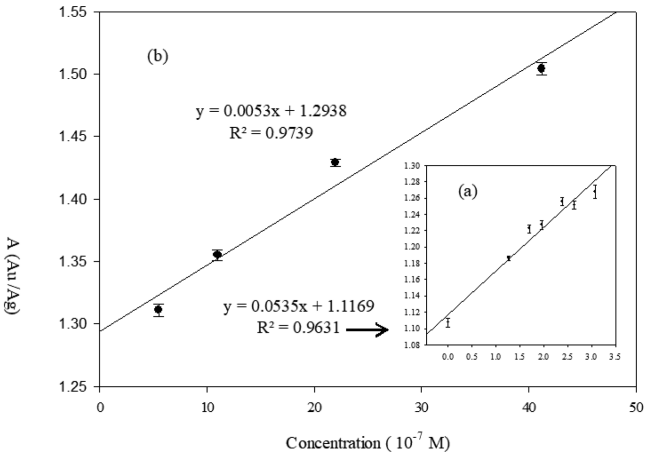

Figure 7. Calibration curve at low (a) and high (b) concentrations.

$\times 10^{-9}$ M with a total time assay of 1 min were obtained (Figure S6 of the Supporting Information).

Detection of HER in Human Serum and Fetal Bovine Serum. Detection capabilities of the LSPR-based probe were tested using human serum and fetal bovine serum. As shown in Table 2, certain amounts of HER were spiked in human serum

Table 2. Detection Capabilities of the LSPR-Based Sensor

sample	added (10^{-8} M)	found (10^{-8} M)	recovery (%)	average RSD (%)
deionized water				
(low concentration)	1.28	1.21	94.53	3.27
	1.96	2.06	105.10	2.80
	2.64	2.51	95.07	2.11
(high concentration)	5.50	5.24	95.27	3.49
	11.00	11.55	105.00	3.12
	41.00	39.66	96.73	2.75
	6.80	7.18	105.58	1.57
human serum	85.00	87.05	102.41	3.27
	170.00	164.57	96.80	4.71
	8.50	8.62	101.41	2.53
fetal bovine serum	68.00	68.34	100.50	2.37
	85.00	88.69	104.34	1.55

(with no dilution with DI) and shook entirely and added to the mixtures of nanoparticles in 0.6 ratios. The obtained calibration curve in serum after one day and 5 days is illustrated in Figures S8 and S9 (in the Supporting Information). When the mixture of human serum, HER, and nanoparticles was stored for 8 days, the nanoparticles settle at the end of microtubes, and the LSPR spectra of solution are decreased with a linear relation in some concentrations. Their corresponding intensities are shown in Table 3. In the next step, the calibration curve in fetal bovine serum via the standard addition method was plotted (Figure S10). The linear range and the slope of the calibration curve in both human serum and fetal bovine serum are approximately similar.

CONCLUSIONS

Determination of HER in biological samples is critical for an efficient diagnosis and screening of HER2-positive breast cancer. The mixture of AuNPs and AgNPs as the sensing reagent can detect HER molecules with an assay time of 1 min via a one-step procedure. The optimization of effective parameters was mathematically measured via CCD under RSM. The linear response range is between 0.5×10^{-7} and 40×10^{-7} M, and the detection limit is 3.7×10^{-9} M. The applicability of the sensor was tested in a human serum sample, and the selectivity was confirmed through the analysis of other possible serum interferences. It is worth noting that the amount of human serum and fetal bovine serum sample required to detect the HER for this homogenous assay is about 37.5 μL. The nanobioassay was verified to be a fast, inexpensive, reliable, and simple analytical tool for quantifying tumor markers in human serum.

ASSOCIATED CONTENT

Supporting Information

The Supporting Information is available free of charge at https://pubs.acs.org/doi/10.1021/acsbiomaterials.1c01369.

Design table, ANOVA table, TEM images of AuNPs, FT-IR spectra of AuNPs and trisodium citrate, XRD pattern of dried powder of AuNPs, optimization value of each parameter, normal plot of residuals, LSPR spectra of the probe in the presence of HER and selected interferences, sensing result during 10 min, AuNP extinction coefficient calculation, calibration curve in plasma after (a) 1 day and (b) 5 days, mixture of plasma, HER, and nanoparticles, and the calibration curve in fetal bovine serum (PDF)

AUTHOR INFORMATION

Corresponding Author

Rouholah Zare-Dorabei − *Research Laboratory of Spectrometry & Micro and Nano Extraction, Department of Chemistry, Iran University of Science and Technology, Tehran 16846-13114, Iran;* orcid.org/0000-0002-4106-9878; Phone: +98 21 77240646; Email: zaredorabei@iust.ac.ir; Fax: +98 21 77491204

Table 3. Comparison of the Reported Assay with Other Studies

sensing material	linear range or the LOD	detection method	refs
core/shell streptavidin-modified CdSe@ZnS quantum dots	0.50−50 ng/mL	electrochemical	12
lead sulfide quantum dot-conjugated secondary HER2 antibody	1−100 ng/mL	electrochemical	50
gold-coated optical fibers	6.6×10^{-7} g/mL	surface plasmon resonance	51
CuO nanoparticles	25 pg./mL to 5 ng/mL	fluorescence ELISA	52
tetrahedral DNA nanostructures (TDNs)	0.1 to 100.0 ng/mL^{-1}	electrochemical	53
aptamer/AuNP	10 nM	colorimetric	54
nanocomplex	24 nM	lateral flow assay	
AuNPs/AgNPs	3.7×10^{-9} M	surface plasmon resonance	present assay

https://doi.org/10.1021/acsbiomaterials.1c01369
ACS Biomater. Sci. Eng. 2022, 8, 871−879

Authors

Neda Shahbazi − *Research Laboratory of Spectrometry & Micro and Nano Extraction, Department of Chemistry, Iran University of Science and Technology, Tehran 16846-13114, Iran*

Seyed Morteza Naghib − *Nanotechnology Department, School of Advanced Technologies, Iran University of Science and Technology, Tehran 16846-13114, Iran*

Complete contact information is available at: https://pubs.acs.org/10.1021/acsbiomaterials.1c01369

Notes

The authors declare no competing financial interest.

■ ACKNOWLEDGMENTS

The author acknowledges financial support from the Iran University of Science and Technology (IUST).

■ ABBREVIATIONS

HER, Herceptin; GNPs, gold nanoparticles; AgNPs, silver nanoparticles; LSPR, localized surface plasmon resonance; RSM, response surface methodology; CCD, central composite design; ECD, extracellular domain; BC, breast cancer; ELISA, enzyme-linked immunosorbent assays; DDW, double-distilled water; RSD, relative standard deviation; TEM, transmission electron microscopy; DLS, dynamic light scattering; FT-IR, Fourier transform infrared; ANOVA, analysis of variance; BSA, bovine serum albumin.

■ REFERENCES

(1) Wei, T.; Xing, H.; Wang, H.; Zhang, Y.; Wang, J.; Shen, J.; Dai, Z. Bovine serum albumin encapsulation of near infrared fluorescent nano-probe with low nonspecificity and cytotoxicity for imaging of HER2-positive breast cancer cells. *Talanta* **2020**, *210*, No. 120625.

(2) Freitas, M.; Neves, M. M. P. S.; Nouws, H. P. A.; Delerue-Matos, C. Quantum dots as nanolabels for breast cancer biomarker HER2-ECD analysis in human serum. *Talanta* **2020**, *208*, No. 120430.

(3) Borghei, Y. S.; Hosseini, M.; Ganjali, M. R.; Hosseinkhani, S. A novel dual-mode and label-free aptasensor based methodology for breast cancer tissue marker targeting. *Sens. Actuators, B* **2020**, *315*, No. 128084.

(4) Emens, L. A.; Esteva, F. J.; Beresford, M.; Saura, C.; De Laurentiis, M.; Kim, S.-B.; Im, S.-A.; Wang, Y.; Salgado, R.; Mani, A.; Shah, J.; Lambertini, C.; Liu, H.; de Haas, S. L.; Patre, M.; Loi, S. Trastuzumab emtansine plus atezolizumab versus trastuzumab emtansine plus placebo in previously treated, HER2-positive advanced breast cancer (KATE2): a phase 2, multicentre, randomised, double-blind trial. *Lancet Oncol.* **2020**, *21*, 1283−1295.

(5) White, B. E.; White, M. K.; Adhvaryu, H.; Makhoul, I.; Nima, Z. A.; Biris, A. S.; Ali, N. Nanotechnology approaches to addressing HER2-positive breast cancer. *Cancer Nanotechnol.* **2020**, *11*, 12.

(6) He, Z.; Chen, Z.; Tan, M.; Elingarami, S.; Liu, Y.; Li, T.; Deng, Y.; He, N.; Li, S.; Fu, J.; Li, W. A review on methods for diagnosis of breast cancer cells and tissues. *Cell Proliferation* **2020**, *53*, e12822.

(7) Wang, Z.; Wang, W.; Bu, X.; Wei, Z.; Geng, L.; Wu, Y.; Dong, C.; Li, L.; Zhang, D.; Yang, S.; Wang, F.; Lausted, C.; Hood, L.; Hu, Z. Microarray Based Screening of Peptide Nano Probes for HER2 Positive Tumor. *Anal. Chem.* **2015**, *87*, 8367−8372.

(8) Altunay, B.; Morgenroth, A.; Beheshti, M.; Vogg, A.; Wong, N. C. L.; Ting, H. H.; Biersack, H.-J.; Stickeler, E.; Mottaghy, F. M. HER2-directed antibodies, affibodies and nanobodies as drug-delivery vehicles in breast cancer with a specific focus on radioimmunotherapy and radioimmunoimaging. *Eur. J. Nucl. Med. Mol. Imaging* **2020**, 1371.

(9) Ahn, S.; Woo, J. W.; Lee, K.; Park, S. Y. HER2 status in breast cancer: changes in guidelines and complicating factors for interpretation. *J. Pathol. Transl. Med.* **2020**, *54*, 34−44.

(10) Sharifi, M.; Hasan, A.; Attar, F.; Taghizadeh, A.; Falahati, M. Development of point-of-care nanobiosensors for breast cancers diagnosis. *Talanta* **2020**, *217*, No. 121091.

(11) Salahandish, R.; Ghaffarinejad, A.; Naghib, S. M.; Majidzadeh-A, K.; Zargartalebi, H.; Sanati-Nezhad, A. Nano-biosensor for highly sensitive detection of HER2 positive breast cancer. *Biosens. Bioelectron.* **2018**, *117*, 104−111.

(12) Freitas, M.; Nouws, H. P. A.; Keating, E.; Fernandes, V. C.; Delerue-Matos, C. Immunomagnetic bead-based bioassay for the voltammetric analysis of the breast cancer biomarker HER2-ECD and tumour cells using quantum dots as detection labels. *Microchim. Acta* **2020**, *187*, 1−10.

(13) Wang, H.-M.; Wang, A.-J.; Yuan, P.-X.; Feng, J.-J. Flower-like metal-organic framework microsphere as a novel enhanced ECL luminophore to construct the coreactant-free biosensor for ultrasensitive detection of breast cancer 1 gene. *Sens. Actuators, B* **2020**, *320*, No. 128395.

(14) Mohammadpour, Z.; Majidzadeh-A, K. Applications of Two-Dimensional Nanomaterials in Breast Cancer Theranostics. *ACS Biomater. Sci. Eng.* **2020**, *6*, 1852−1873.

(15) Sha, Q.; Guan, R.; Su, H.; Zhang, L.; Liu, B.-F.; Hu, Z.; Liu, X. Carbohydrate-protein template synthesized high mannose loading gold nanoclusters: A powerful fluorescence probe for sensitive Concanavalin A detection and specific breast cancer cell imaging. *Talanta* **2020**, *218*, No. 121130.

(16) Yang, J.; Wang, T.; Zhao, L.; Rajasekhar, V. K.; Joshi, S.; Andreou, C.; Pal, S.; Hsu, H.-T.; Zhang, H.; Cohen, I. J. Gold/alpha-lactalbumin nanoprobes for the imaging and treatment of breast cancer. *Nat. Biomed. Eng.* **2020**, *4*, 686−703.

(17) Tanaka, S.-I.; Wadati, H.; Sato, K.; Yasuda, H.; Niioka, H. Red-Fluorescent Pt Nanoclusters for Detecting and Imaging HER2 in Breast Cancer Cells. *ACS Omega* **2020**, *5*, 23718−23723.

(18) Zhang, X.; Chen, M.; Zhang, Y.; Hou, Y.; Wu, Y.; Yao, M.; Li, L.; Shi, L.; Liu, T.; Hu, B. Monoclonal-Antibody-Templated Gold Nanoclusters for HER2 Receptors Targeted Fluorescence Imaging. *ACS Appl. Bio Mater.* **2020**, *3*, 7061−7066.

(19) Li, N.; Zong, S.; Zhang, Y.; Wang, Z.; Wang, Y.; Zhu, K.; Yang, K.; Wang, Z.; Chen, B.; Cui, Y. A SERS-colorimetric dual-mode aptasensor for the detection of cancer biomarker MUC1. *Anal. Bioanal. Chem.* **2020**, *412*, 5707−5718.

(20) Leyland-Jones, B. Trastuzumab: hopes and realities. *Lancet Oncol.* **2002**, *3*, 137−144.

(21) Cathcart, N.; Chen, J. I. L. Sensing biomarkers with plasmonics. *Anal. Chem.* **2020**, 7373.

(22) Bai, Y.; Li, H.; Xu, J.; Huang, Y.; Zhang, X.; Weng, J.; Li, Z.; Sun, L. Ultrasensitive colorimetric biosensor for BRCA1 mutation based on multiple signal amplification strategy. *Biosens. Bioelectron.* **2020**, *166*, No. 112424.

(23) Miti, A.; Thamm, S.; Müller, P.; Csáki, A.; Fritzsche, W.; Zuccheri, G. A miRNA biosensor based on localized surface plasmon resonance enhanced by surface-bound hybridization chain reaction. *Biosens. Bioelectron.* **2020**, *167*, No. 112465.

(24) Tian, L.; Qian, K.; Qi, J.; Liu, Q.; Yao, C.; Song, W.; Wang, Y. Gold nanoparticles superlattices assembly for electrochemical biosensor detection of microRNA-21. *Biosens. Bioelectron.* **2018**, *99*, 564−570.

(25) Cui, A.; Zhang, J.; Bai, W.; Sun, H.; Bao, L.; Ma, F.; Li, Y. Signal-on electrogenerated chemiluminescence biosensor for ultrasensitive detection of microRNA-21 based on isothermal strand-displacement polymerase reaction and bridge DNA-gold nanoparticles. *Biosens. Bioelectron.* **2019**, *144*, No. 111664.

(26) Hakimian, F.; Ghourchian, H.; Sadat Hashemi, A.; Arastoo, M. R.; Rad, M. B. Ultrasensitive optical biosensor for detection of miRNA-155 using positively charged Au nanoparticles. *Sci. Rep.* **2018**, *8*, 1−9.

(27) Dong, W.; Ren, Y.; Bai, Z.; Yang, Y.; Chen, Q. Fabrication of hexahedral Au-Pd/graphene nanocomposites biosensor and its application in cancer cell H2O2 detection. *Bioelectrochemistry* **2019**, *128*, 274−282.
(28) Choi, N.; Dang, H.; Das, A.; Sim, M.; Chung, I. Y.; Choo, J. SERS biosensors for ultrasensitive detection of multiple biomarkers expressed in cancer cells. *Biosens. Bioelectron.* **2020**, *164*, No. 112326.
(29) Afzalinia, A.; Mirzaee, M. Ultrasensitive Fluorescent miRNA Biosensor Based on a "Sandwich" Oligonucleotide Hybridization and Fluorescence Resonance Energy Transfer Process Using an Ln (III)-MOF and Ag Nanoparticles for Early Cancer Diagnosis: Application of Central Composite Design. *ACS Appl. Mater. Interfaces* **2020**, *12*, 16076−16087.
(30) Salahandish, R.; Ghaffarinejad, A.; Omidinia, E.; Zargartalebi, H.; Majidzadeh-A, K.; Naghib, S. M.; Sanati-Nezhad, A. Label-free ultrasensitive detection of breast cancer miRNA-21 biomarker employing electrochemical nano-genosensor based on sandwiched AgNPs in PANI and N-doped graphene. *Biosens. Bioelectron.* **2018**, *120*, 129−136.
(31) Dong, W.; Ren, Y.; Bai, Z.; Yang, Y.; Wang, Z.; Zhang, C.; Chen, Q. Trimetallic AuPtPd nanocomposites platform on graphene: Applied to electrochemical detection and breast cancer diagnosis. *Talanta* **2018**, *189*, 79−85.
(32) Wang, Y.; Zhu, G.; Qi, W.; Li, Y.; Song, Y. A versatile quantitation platform based on platinum nanoparticles incorporated volumetric bar-chart chip for highly sensitive assays. *Biosens. Bioelectron.* **2016**, *85*, 777−784.
(33) Thakor, A. S.; Jokerst, J.; Zavaleta, C.; Massoud, T. F.; Gambhir, S. S. Gold Nanoparticles: A Revival in Precious Metal Administration to Patients. *Nano Lett.* **2011**, *11*, 4029−4036.
(34) Loyez, M.; Hassan, E. M.; Lobry, M.; Liu, F.; Caucheteur, C.; Wattiez, R.; DeRosa, M. C.; Willmore, W. G.; Albert, J. Rapid detection of circulating breast cancer cells using a Multiresonant optical fiber Aptasensor with plasmonic amplification. *ACS Sens.* **2020**, *5*, 454−463.
(35) Ranjan, P.; Parihar, A.; Jain, S.; Kumar, N.; Dhand, C.; Murali, S.; Mishra, D.; Sanghi, S. K.; Chaurasia, J. P.; Srivastava, A. K. Biosensor-based diagnostic approaches for various cellular biomarkers of breast cancer: A comprehensive review. *Anal. Biochem.* **2020**, *610*, No. 113996.
(36) Shahbazi, N.; Zare-Dorabei, R. A Facile Colorimetric and Spectrophotometric Method for Sensitive Determination of Metformin in Human Serum Based on Citrate-Capped Gold Nanoparticles: Central Composite Design Optimization. *ACS Omega* **2019**, *4*, 17519−17526.
(37) Zeineldin, R., 10 - Nanotechnology for cancer screening and diagnosis: from innovations to clinical applications. *In Biomaterials for Cancer Therapeutics*, 2nd ed.; Park, K., Ed.; Woodhead Publishing, 2020; pp 261−289.
(38) Wang, K.; Zhang, F.; Wei, Y.; Wei, W.; Jiang, L.; Liu, Z.; Liu, S. In Situ Imaging of Cellular Reactive Oxygen Species and Caspase-3 Activity Using a Multifunctional Theranostic Probe for Cancer Diagnosis and Therapy. *Anal. Chem.* **2021**, *93*, 7870.
(39) Wang, K.; Jiang, L.; Zhang, F.; Wei, Y.; Wang, K.; Wang, H.; Qi, Z.; Liu, S. Strategy for in situ imaging of cellular alkaline phosphatase activity using gold nanoflower probe and localized surface plasmon resonance technique. *Anal. Chem.* **2018**, *90*, 14056−14062.
(40) Wang, K.; Shangguan, L.; Liu, Y.; Jiang, L.; Zhang, F.; Wei, Y.; Zhang, Y.; Qi, Z.; Wang, K.; Liu, S. In situ detection and imaging of telomerase activity in cancer cell lines via disassembly of plasmonic core−satellites nanostructured probe. *Anal. Chem.* **2017**, *89*, 7262−7268.
(41) Wu, T.; Ge, Z.; Liu, S. Fabrication of thermoresponsive cross-linked poly (N-isopropylacrylamide) nanocapsules and silver nanoparticle-embedded hybrid capsules with controlled shell thickness. *Chem. Mater.* **2011**, *23*, 2370−2380.
(42) Shahbazi, N.; Zare-Dorabei, R.; Naghib, S. M. Multifunctional nanoparticles as optical biosensing probe for breast cancer detection: A review. *Mater. Sci. Eng., C* **2021**, *127*, No. 112249.
(43) Wu, T.; Zhang, Q.; Hu, J.; Zhang, G.; Liu, S. Composite silica nanospheres covalently anchored with gold nanoparticles at the outer periphery of thermoresponsive polymer brushes. *J. Mater. Chem.* **2012**, *22*, 5155−5163.
(44) Yao, C.; Li, Y.; Wang, Z.; Song, C.; Hu, X.; Liu, S. Cytosolic NQO1 enzyme-activated near-infrared fluorescence imaging and photodynamic therapy with polymeric vesicles. *ACS Nano* **2020**, *14*, 1919−1935.
(45) Hu, X.; Liu, S. Recent advances towards the fabrication and biomedical applications of responsive polymeric assemblies and nanoparticle hybrid superstructures. *Dalton Trans.* **2015**, *44*, 3904−3922.
(46) Wulandari, P.; Nagahiro, T.; Fukada, N.; Kimura, Y.; Niwano, M.; Tamada, K. Characterization of citrates on gold and silver nanoparticles. *J. Colloid Interface Sci.* **2015**, *438*, 244−248.
(47) Frost, M. S.; Dempsey, M. J.; Whitehead, D. E. The response of citrate functionalised gold and silver nanoparticles to the addition of heavy metal ions. *Colloids Surf., A* **2017**, *518*, 15−24.
(48) Cardinali, B.; Lunardi, G.; Millo, E.; Armirotti, A.; Damonte, G.; Profumo, A.; Gori, S.; Iacono, G.; Levaggi, A.; Del Mastro, L. Trastuzumab quantification in serum: a new, rapid, robust ELISA assay based on a mimetic peptide that specifically recognizes trastuzumab. *Anal. Bioanal. Chem.* **2014**, *406*, 4557−4561.
(49) Jamieson, D.; Cresti, N.; Verrill, M. W.; Boddy, A. V. Development and validation of cell-based ELISA for the quantification of trastuzumab in human plasma. *J. Immunol. Methods* **2009**, *345*, 106−111.
(50) Lah, Z. M. A. N. H.; Ahmad, S. A. A.; Zaini, M. S.; Kamarudin, M. A. An Electrochemical Sandwich Immunosensor for the Detection of HER2 using Antibody-Conjugated PbS Quantum Dot as a label. *J. Pharm. Biomed. Anal.* **2019**, *174*, 608−617.
(51) Loyez, M.; Lobry, M.; Hassan, E. M.; DeRosa, M. C.; Caucheteur, C.; Wattiez, R. HER2 breast cancer biomarker detection using a sandwich optical fiber assay. *Talanta* **2021**, *221*, No. 121452.
(52) Tian, S.; Zeng, K.; Yang, A.; Wang, Q.; Yang, M. A copper based enzyme-free fluorescence ELISA for HER2 detection. *J. Immunol. Methods* **2017**, *451*, 78−82.
(53) Ou, D.; Sun, D.; Lin, X.; Liang, Z.; Zhong, Y.; Chen, Z. A dual-aptamer-based biosensor for specific detection of breast cancer biomarker HER2 via flower-like nanozymes and DNA nanostructures. *J. Mater. Chem. B* **2019**, *7*, 3661−3669.
(54) Ranganathan, V.; Srinivasan, S.; Singh, A.; DeRosa, M. C. An aptamer-based colorimetric lateral flow assay for the detection of human epidermal growth factor receptor 2 (HER2). *Anal. Biochem.* **2020**, *588*, No. 113471.

https://doi.org/10.1021/acsbiomaterials.1c01369
ACS Biomater. Sci. Eng. 2022, 8, 871−879